Effects of Including an N-Terminal Insertion Region and Arginine-Mimetic Side Chains in Helical Peptoid Analogues of Lung Surfactant Protein B[†]

Shannon L. Seurynck-Servoss,[‡] Michelle T. Dohm,[§] and Annelise E. Barron*,[‡]

Department of Chemical and Biological Engineering and Department of Chemistry, Northwestern University, 2145 Sheridan Road, Evanston, Illinois 60208

Received March 28, 2006; Revised Manuscript Received August 9, 2006

ABSTRACT: Surfactant protein B (SP-B) is one of two helical, amphipathic proteins critical for the biophysical functioning of lung surfactant (LS) and hence is an important therapeutic protein. This small, complex 79mer has three internal disulfide bonds and homodimerizes via another disulfide bridge. A helical, amphipathic 25mer from the amino terminus (SP-B$_{1-25}$) exhibits surface-active properties similar to those of full-length, synthetic SP-B. In previous work, we created helical, non-natural mimics of SP-B$_{1-25}$ based on sequence-specific peptoid 17mers and demonstrated their biomimetic surface activity. Like SP-B$_{1-25}$, the peptoids were designed to adopt helical structures with cationic and nonpolar faces. Here, we compare the surface activities of six different helical peptoid analogues of SP-B$_{1-25}$ to investigate the importance of mimicking its N-terminal insertion domain as well as its two arginine residues, both thought to be important for the peptide's proper function. Although the peptoid analogues of SP-B$_{1-25}$ studied here share many similar features and all functionally mimic SP-B$_{1-25}$ to some degree, it is notable that small differences in their sequences and side chain chemistries lead to substantial differences in their observed interactions with a lipid film. A peptoid comprising a hydrophobic, helical insertion region with aromatic side chains shows more biomimetic surface activity than simpler peptoids, and even better activity, by comparison to natural LS, than SP-B$_{1-25}$. However, the substitution of lysine-like side chains for arginine-like side chains in the peptoid has little effect on biomimetic surface activity, indicating that interactions of the guanidino groups with lipids may not be critical for the function of these SP-B mimics.

In this paper, we investigate a new family of non-natural peptoid analogues of surfactant protein B (SP-B), an important protein in lung surfactant (LS) replacements used to treat respiratory distress syndrome (RDS). RDS occurs in premature infants that are not yet able to secrete functional LS into alveolar spaces, leading to difficulty breathing and ultimately to death. Current treatment involves the instillation of an animal-derived LS replacement through the trachea in two to four doses over several days. While animal-derived replacements are quite effective for the treatment of RDS, they are expensive due to complex isolation techniques and batch-to-batch variability, there are difficulties in large-scale production and suspension techniques, and there is a risk of immune response as well as a possibility of transspecies pathogen transmission (*1−3*). Entirely synthetic LS replacements developed to date, which contain lipids and synthetic spreading agents, are less expensive and more safe but have relatively poor in vivo efficacy compared to that of natural LS, primarily due to their lack of the hydrophobic surfactant proteins (SPs) that are required for proper LS function (*2*).

The main surface activities required for a functional LS replacement are (i) rapid adsorption to the air−liquid interface, (ii) attainment of near-zero surface tension upon surfactant film compression, and (iii) negligible loss of surfactant material from the interface upon multiple expansions and compressions (*4*). A biomimetic LS replacement containing lipids and functional mimics of the hydrophobic SPs would ideally retain the excellent efficacy of the natural material but have the better bioavailability, safety, and relatively low cost per dose of the synthetic surfactant.

LS is a complex mixture of biomolecules that coats the interior surfaces of alveoli and is responsible for the regulation of surface tension in the lung, reducing the work of breathing and stabilizing alveolar structures. It is composed of approximately 90% lipids and 10% surfactant proteins. The main lipid component, dipalmitoylphosphatidylcholine (DPPC), forms a tightly packed monolayer that is able to reach near-zero surface tension upon compression but does not rapidly adsorb to the interface and exhibits poor respreadability (i.e., sustains a large loss of material during compression and expansion of the film area) (*2, 5, 6*). Other lipids present in LS include unsaturated phospholipids such as palmitoleoylphosphatidylglycerol (POPG) and many others. Addition of POPG and/or fatty acids such as palmitic acid (PA) to DPPC leads to more rapid adsorption and better respreadability of the lipid film, but this type of mixed-lipid film fails to reach near-zero surface tension upon compression (*7*).

* To whom correspondence should be addressed: Department of Chemical and Biological Engineering, Northwestern University, 2145 Sheridan Rd., Evanston, IL 60208. Phone: (847) 491-2778. Fax: (847) 491-3728. E-mail: a-barron@northwestern.edu.
[‡] Department of Chemical and Biological Engineering.
[§] Department of Chemistry.

Of the four proteins found in native LS, the hydrophobic SPs, SP-B and SP-C, are the two primarily involved in facilitating the proper lipid film dynamics for regulation of the surface tension at the alveolar air−liquid interface (*1*, *2*, *5*, *8*, *9*). Both SP-B and SP-C are predominantly helical in structure (*2*) and contain cationic residues that interact with anionic lipid head groups (*2*, *10*). Both proteins are highly conserved among mammalian species (*1*, *2*), but SP-B plays a significant role in the processing of SP-C; while SP-B knockout mice die shortly after birth (*11*), SP-C knockout mice are able to survive with decreased lung function (*12*). SP-B comprises 79 amino acid residues, with seven cysteines that form three intramolecular disulfide bonds and one intermolecular disulfide bond, leading to homodimer formation (*2*, *13*−*16*). SP-B also possesses four to five amphipathic helices that have been shown to interact with and perturb lipid membranes. It is hypothesized that SP-B regulates surface tension through its involvement in the stabilization and organization of the lipid film (*2*, *17*), thereby improving monolayer adsorption and respreading during respiration (*2*, *18*). It has also been suggested that SP-B is responsible for the selective removal of non-DPPC lipids from the film upon compression (*17*, *19*).

Although synthesizing and obtaining the proper folding of a mimic of this 79mer are quite difficult, studies have shown that a segment from the N-terminus, SP-B$_{1-25}$, has surface-active behavior similar to that of the full-length protein (*20*−*23*). Residues 1−9 form a proline-rich, flexible domain termed "the insertion region", which has recently been shown to be critical for SP-B's surface tension reducing properties. Amino acid substitutions for tryptophan 9 or prolines 2, 4, and 6 markedly decreased the surface activity of N-terminal SP-B peptide mimics (*24*, *25*). SP-B's insertion region is hypothesized to insert into the lipid layer and interact with the hydrophobic lipid tails, while the attached amphipathic helix orients itself to interact with both the charged lipid head groups and the acyl chains, thus facilitating lipid transport and organization (*26*, *27*). Atomistic molecular dynamic simulations of SP-B$_{1-25}$ in either a DPPC or DPPG monolayer support this claim (*28*). The two lysine and two arginine residues in the amphipathic helix of SP-B$_{1-25}$ also contribute significantly to its surface activity. Previous work has indicated that the presence of arginine rather than lysine is critical for lipid−protein interactions, where SP-B$_{1-25}$ modeled in a DPPG monolayer predicts that arginine 12 interacts strongly with the anionic head groups; it is also found to interact with the zwitterionic DPPC head groups, but to a lesser extent. Thus, the type and distribution of basic residues along the polar face of the amphipathic helix may be of great importance to the surface activity of SP-B.

While peptide mimics of SP-B that include these structural attributes have exhibited good in vitro and in vivo efficacy, they are expensive to synthesize and are susceptible to protease degradation. Non-natural molecules such as poly-N-substituted glycines, or peptoids, offer an alternative backbone that is not degraded by proteases (*29*, *30*) and therefore are promising for therapeutic use. Peptoids have several advantages, including the fact that they are easily synthesized on a solid support using the submonomer protocol developed by Zuckermann et al. (*30*). The peptoid side chains are attached at the amide nitrogen rather than

the α-carbon, rendering the backbone achiral with no hydrogen bond donors. Despite these characteristics, peptoids with α-chiral side chains are able to form stable helices with a single handedness. NMR studies of a peptoid pentamer with bulky chiral side chains revealed that the structure was a polyproline type I-like helix (*31*).

In previous work, we studied the relative surface activities of three facially amphipathic, cationic peptoid mimics of SP-B$_{1-25}$ that had simple, repetitive sequences but which exhibited varying helicities and hydrophobicities. The promise of the peptoid-based SP mimics was judged by making a direct comparison of surface activity to that of the SP-B$_{1-25}$ peptide in a lipid mixture which mimics that found in natural LS (*32*). We performed in vitro characterization of the various surfactant films using a Langmuir−Wilhelmy surface balance (LWSB) with epifluorescent microscopic imaging of film phase morphology, as well as a pulsating bubble surfactometer (PBS). Our study showed that one of the peptoid 17mers exhibited surface-active behavior similar to and, in some ways, superior to that of the SP-B$_{1-25}$ peptide. In the study presented here, we have designed four new peptoid-based mimics of SP-B$_{1-25}$ that possess a greater degree of sequence similarity to the natural peptide than our previous designs, specifically including a hydrophobic N-terminal insertion region and biomimetic placement of arginine- and/or lysine-like side chains on two faces of the helix rather than on one face (as in the previously studied peptoids). The surface-active behaviors of the peptoid-based SP-B mimics were characterized in a lipid film using both an LWSB and a modified PBS that provides accurate measurements of dynamic surface tension by direct bubble imaging (*33*). The results show that the inclusion of an N-terminal insertion region leads to a substantial improvement in the surface-active behavior of the peptoid-based mimic and that the substitution of lysine-like side chains for arginine-like side chains in the peptoid helix has little to no effect on surface activity.

MATERIALS AND METHODS

Materials. Peptide and peptoid synthesis reagents were purchased from Applied Biosystems (Foster City, CA) and Aldrich (Milwaukee, WI). Resins and Fmoc-protected amino acids were purchased from NovaBiochem (San Diego, CA); 2,2,5,7,8-pentamethylchroman-6-sulfonyl chloride (PMC) was purchased from Omega Chemical (Quebec, CA), and primary amines and di-*tert*-butyl dicarbonate (Boc) were purchased from Aldrich. Acetonitrile and trifluoroacetic acid were purchased from Fisher Scientific (Pittsburgh, PA). DPPC and POPG were purchased from Avanti Polar Lipids (Alabaster, AL), and PA was purchased from Aldrich. All chemicals were used without further purification.

Peptide and Peptoid Synthesis, Purification, and Characterization. The modified SP-B$_{1-25}$ peptide was synthesized by Fmoc chemistry on preloaded Wang resin using an ABI 433A automated peptide synthesizer (Applied Biosystems). Peptoids were synthesized using an ABI 433A automated peptide synthesizer on Rink amide resin by the submonomer protocol (*30*), with Boc protection of NLys (*34*) and PMC protection of NArg (*35*). All molecules were cleaved from the resin with trifluoroacetic acid in the presence of the appropriate scavenging reagents for 2−10 min or 1 h (the

Table 1: SP-B Mimic Sequences, Molar Masses, and % HPLC Elution

Oligomer	Monomer sequence (amino to carboxy)†	Molar Mass (Da)	% HPLC Elution
SP-B$_{1-25}$ (C8→A, C11→A)	FPIPLPYAWLA**R**ALI**KR**IQAMIP**K**G	2865	56
Peptoid **B1**	*N*spe-*N*spe-(**N**Lys-*N*spe-*N*spe)$_5$	2592	53
Peptoid **B2**	*N*spe$_8$-**N**Arg-*N*spe$_2$-**N**Lys-**N**Arg-*N*spe$_4$-**N**Lys-*N*spe$_2$	3165	Not determined
Peptoid **B3**	*N*spe$_8$-**N**Lys-*N*spe$_2$-**N**Lys-**N**Lys-*N*spe$_4$-**N**Lys-*N*spe$_2$	3108	56
Peptoid **B4**	*N*ssb-*N*ssb-(**N**Lys-*N*ssb-*N*ssb)$_5$	2016	39
Peptoid **B5**	*N*ssb$_8$-**N**Arg-*N*ssb$_2$-**N**Lys-**N**Arg-*N*ssb$_4$-**N**Lys-*N*ssb$_2$	2396	50
Peptoid **B6**	*N*ssb$_8$-**N**Lys-*N*ssb$_2$-**N**Lys-**N**Lys-*N*ssb$_4$-**N**Lys-*N*ssb$_2$	2340	58

† Cationic side chains are highlighted in red; NArg side chains are highlighted in purple.

longer time was necessary for the removal of the PMC protecting group). Peptoids were purified by reversed phase high-performance liquid chromatography (RP-HPLC) on a Vydac C4 column (catalog no. 214TP101550) using a linear gradient from 20 to 95% solvent B in solvent A over 50 min [solvent A is 0.1% TFA in water (v/v), and solvent B is 0.1% TFA in acetonitrile (v/v)]. Final purities were confirmed to be >97% by analytical RP-HPLC on a Vydac C4 column (catalog no. 214TP53), and molecular weights were confirmed by electrospray ionization mass spectrometry (Table 1).

Sample Preparation. DPPC, POPG, and PA were individually dissolved in chloroform and methanol (3/1, v/v) to a known concentration (~4 mg/mL). Lipids were then combined at a 68/22/9 (w/w) DPPC/POPG/PA ratio to a total lipid concentration of ~2 mg/mL. This lipid formulation has previously been shown to be a good mimic of the nonprotein fraction of LS (*36*). The peptoids and SP-B$_{1-25}$ peptide were dissolved in methanol to a known concentration (~2 mg/mL) and then added to the lipid mixture at 2.16 mol % (equivalent to 10 wt % SP-B$_{1-25}$), resulting in a final concentration of ~1 mg of lipid/mL.

Circular Dichroism. Circular dichroism (CD) spectroscopy studies were performed at room temperature in methanol at a concentration of ~60 μM. CD spectra were obtained using a Jasco J-715 instrument and a cylindrical quartz cuvette (Hellma, Plainview, NY) with a path length of 0.02 cm. Each spectrum represents the average of 40 successive accumulations.

Langmuir–Wilhelmy Surface Balance Studies. Surface pressure–molecular area isotherms were obtained using a custom-built Langmuir–Wilhelmy surface balance, previously described elsewhere (*32*). The Teflon trough was filled with 300 mL of buffer [150 mM NaCl, 5 mM CaCl$_2$, and 10 mM HEPES (pH 6.9)] and heated to 37 °C. The surfactant formulation was spread at the air–liquid interface from a chloroform/methanol solution using a glass syringe; solvent was allowed to evaporate over 5 min. The two Teflon barriers were then compressed and expanded and then compressed at a rate of 30 mm/min. Surface pressure was measured

throughout the experiment using a Wilhelmy plate (Riegler and Kirsten GMBH, Berlin, Germany). Experiments were repeated for a total of six times for each formulation and were reproducible.

Pulsating Bubble Surfactometry. A modified pulsating bubble surfactometer (General Transco, Largo, FL), previously described elsewhere (*33*), was used to obtain both static-bubble and dynamic-bubble adsorption data. An image acquisition system has been added to the commercial PBS to allow for accurate tracking of bubble shape and size in real time. Images and pressure data from the instrument are sent to a custom-designed LabVIEW program that is used to fit the bubble to an ellipse and calculate both the surface tension and the surface area of the bubble (*33*). Some of the major differences observed with the image analysis system as compared to the commercial PBS include generally higher maximum surface tensions, reduced hysteresis in the data loop, and a reduced slope upon expansion of the bubble.

Surfactant formulations were dried from the chloroform/methanol solution using a DNA 120 Speedvac (Thermo Electron, Holbrook, NY), forming a pellet. The pellet was suspended in aqueous buffer [150 mM NaCl, 5 mM CaCl$_2$, and 10 mM HEPES (pH 6.9)] to 1.0 mg of lipid/mL, with a final volume of ~70 μL. The surfactant formulations were mixed with a pipet, sonicated with a Fisher model 60 probe sonicator, and then mixed with a pipet again to form a uniform suspension. Samples were loaded into a sample chamber (General Transco) with putty placed on the capillary end of the sample chamber; the putty was removed before experiments were performed. A similar method has previously been shown to prevent leakage of the sample into the capillary (*37*). All experiments were conducted at 37 °C. Static adsorption data were collected for 20 min or until equilibrium surface tension was reached, starting with a bubble radius of 0.4 mm without adjustment of bubble size throughout the experiment. Dynamic adsorption data were obtained at a frequency of 20 cycles/min (similar to the adult breathing rate) until equilibrium was reached following static
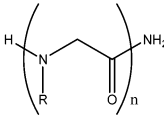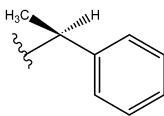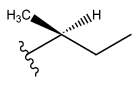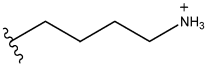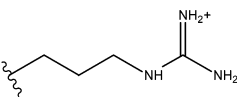
adsorption, again starting with a minimum bubble radius of 0.4 mm without adjustment of bubble size throughout the experiment. For both static- and dynamic-bubble experiments, equilibrium was defined as the point at which the minimum and maximum surface tension remained constant for >2 min. PBS experiments were repeated for a total of six times for each surfactant formulation and were reproducible.

RESULTS AND DISCUSSION

Peptoid Sequence Design Rationale. It has been shown that a short, 25mer segment from the N-terminus (SP-B$_{1-25}$) retains much of the surface-active behavior of full-length SP-B (*20–23*). We are working to mimic this helical, amphipathic peptide using peptoids, which are synthesized in high yield and are protease-resistant and easy to design for helical and amphipathic structure. In a previous study, we showed that peptoid-based mimics of SP-B with simple, repetitive sequences and stable helical structures had surface-active behavior comparable to that of the control peptide, SP-B$_{1-25}$ (*32*). The three peptoids previously investigated contained lysine-like side chains incorporated at every third position, resulting in one cationic face on the peptoid helix, and either aromatic or aliphatic, chiral hydrophobic side chains at the remaining two positions, leading to two nonpolar faces. The most hydrophobic and helical peptoid, containing two-thirds chiral, aromatic, phenylalanine-like side chains, called in this paper peptoid **B1**, was the most surface-active. The peptoid with the most "biomimetic" sequence, called **B4**, which comprised two-thirds chiral, aliphatic, isoleucine-like side chains, was the least surface-active. These peptoids had simple, repetitive sequences, and although they mimicked the amphipathic helical structure of SP-B residues 8–22 well, we found that they did not exhibit all of the surface-active behaviors exhibited by SP-B$_{1-25}$. Specifically, the simple peptoids we studied previously had slightly later lift-off molecular areas, as determined on the LWSB, and higher maximum surface tensions, as determined in dynamic-bubble PBS studies. We concluded that these simple, helical peptoids were lacking some of the essential structural features displayed by SP-B$_{1-25}$.

In particular, the hydrophobic, N-terminal insertion region and the two arginine residues present within the amphipathic helix are structural features that may be important for the biophysical functioning of SP-B$_{1-25}$ (*28, 38*). In addition, the cationic residues of SP-B$_{1-25}$ are distributed over two faces of the helix as opposed to just one face, as was the case for the first generation of simple peptoid-based mimics. While retaining the aromatic side chain content of **B1**, which was previously our most promising compound, we have now designed a peptoid that incorporates both of these features (**B2**, Table 1). Peptoid **B2** comprises an octameric, hydrophobic, helical insertion region at the N-terminus and has biomimetic placement of two arginine-like side chains (NArg) as well as two lysine-like side chains (NLys) that form two partially cationic faces in the C-terminal helix (side chain structures shown in Table 2). The remaining side chains in the C-terminal helix are the hydrophobic, chiral, and aromatic Nspe side chains, forming one entirely hydrophobic face. While this peptoid was synthesized, we found that it was not possible to purify the desired product in good yield due to difficulties with peptoid cleavage and degradation.

Table 2: N-Substituted Glycine Side Chain Structures

R = side chain	Designator
	*N*spe = (*S*)-*N*-(1-phenylethyl)glycine
	*N*ssb = (*S*)-*N*-(2-butyl)glycine
	*N*Lys = *N*-(4-aminobutyl)glycine
	*N*Arg = *N*-(3-guanidinopropyl)glycine

The inclusion of NArg side chains in peptoids is problematic for two reasons: (1) The PMC-protected amine has low solubility in solvents used for peptoid synthesis, leading to a low coupling efficiency, and (2) extended cleavage times are required for the removal of PMC, which can lead to acid-induced degradation of peptoid monomers with Nspe side chains. For **B2**, the long cleavage required to remove PMC resulted in substantial cleavage of the Nspe side chains, and the desired compound could not be isolated in sufficient yield for study.

We therefore designed a peptoid that substituted NLys side chains for the NArg side chains (**B3**, Table 1). The protected NLys submonomer (mono-Boc-diaminobutane) is much easier to use than NArg, and we hypothesized that substitution of NArg for NLys would make little difference in the overall in vitro surface activity. Consequently, peptoids **B5** and **B6** (Table 1) were designed to determine whether this substitution affected surface activity. The sequence of **B5** is based on that of **B2**, while that of **B6** is based on that of **B3**; in both cases, all Nspe side chains were substituted with Nssb side chains. The hydrophobic side chains used in these peptoids hence are the same as those included in the least surface-active peptoid from our previous paper, **B4**. The Nssb side chain is not acid-labile and can withstand the long cleavage times required for removal of the PMC protecting group. Therefore, we were able to purify **B5** in good yield, allowing us to determine the importance of the arginine-like side chain in peptoid mimics. Table 1 presents data on the relative lipophilicity of the studied peptoid analogues, in terms of the percentage acetonitrile at which they elute from an analytical RP-HPLC column with C4 packing. Due to differences in the hydrophobic side chain chemistries of the various peptoid oligomers, the hydrophobicity of the peptoids, relative to the control peptide, varied as follows: **B6** > **B3** ~ SP-B$_{1-25}$ > **B1** > **B5** ≫ **B4**. Properties of the novel, more biomimetic peptoid sequences **B3**, **B5**, and **B6**
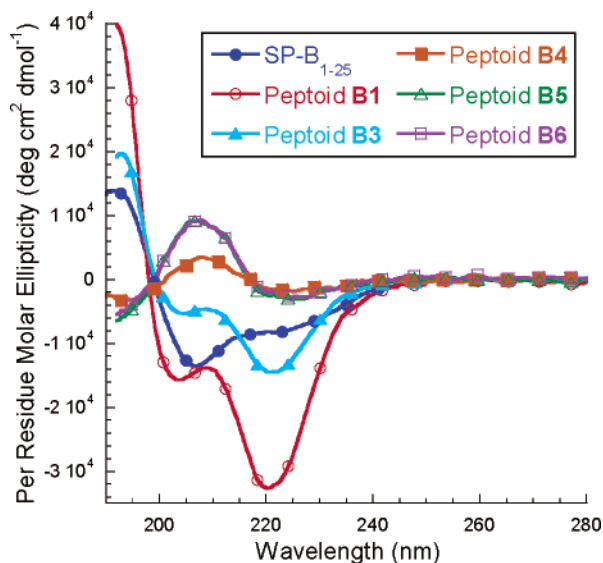
FIGURE 1: CD spectra of SP-B$_{1-25}$ (blue, filled circles), peptoid **B1** (red, empty circles), peptoid **B3** (light blue, filled triangles), peptoid **B4** (orange, filled squares), peptoid **B5** (green, empty triangles), and peptoid **B6** (purple, empty squares) in methanol.

were compared to those of two of the simple, helical peptoids from the previous study [**B1**, which has two-thirds chiral, aromatic, Nspe side chains; and **B4**, which has two-thirds chiral, aliphatic, Nssb side chains (*32*)] and a modified peptide mimic of SP-B$_{1-25}$ with cysteine-to-alanine substitutions that prevent the formation of unwanted disulfide bonds (*21*) (Table 1).

Circular Dichroism Spectroscopy. Circular dichroism spectroscopy (CD) was performed in methanol at room temperature (Figure 1). All peptide- and peptoid-based mimics have CD spectra that exhibit spectral features indicative of helical structure. The spectrum for SP-B$_{1-25}$ has a maximum at ~195 nm and two minima at ~205 and ~220 nm, as expected for a peptide α-helix. The spectra for **B1** and **B3** are similar, each with a maximum at ~192 nm and two minima at ~205 and ~220 nm, which is indicative of a polyproline type I-like peptoid helix (*31, 39–41*). This result is similar to CD spectra previously published for other peptoids containing chiral, aromatic side chains (*31, 39–41*), as well as for **B1** (*32*), which reveals a very stable helix. **B4**, **B5**, and **B6** all have spectra similar to that observed for a peptide polyproline type I helix, with a single maximum at ~205 nm and two shallow minima at ~190 and ~225 nm; this is also indicative of a peptoid polyproline type I-like helix (*41, 42*). These CD spectra are similar to those previously published for peptoids with chiral, aliphatic side chains (*41, 42*) and for **B4** (*32*) and reveal a helix that is less stable than those formed by **B1** and **B3**. The spectra for both **B5** and **B6** nearly overlay one another, which is expected because the substitution of lysine for arginine is not expected to affect secondary structure to a significant degree. **B5** and **B6** also have more intense spectra than **B4**, indicative of a more stable helix. This is due to the higher percentage of chiral side chains (80% vs 70%) in **B5** and **B6** as compared to that in **B4**, which leads to a more stable helical structure (*41*).

Langmuir–Wilhelmy Surface Balance Surfactometry. A Langmuir–Wilhelmy surface balance (LWSB) was used to obtain surface pressure versus molecular area isotherms at

37 °C for all surfactant formulations (Figure 2). In a typical LWSB experiment, the surfactant is spread at the air–buffer interface at a concentration such that the lipids are in the gaseous surface phase, where the molecules are not significantly interacting with one another. As the barriers are compressed, the molecules are brought closer together and the lipid tails begin to interact with one another and enter the liquid expanded (LE) phase, corresponding to an observable increase in surface pressure (commonly termed the lift-off area). A good LS replacement is expected to have a high lift-off area (>100 Å^2/molecule) (*43*). As the barriers are further compressed, a change in the slope of the isotherm is observed at ~25 mN/m, corresponding to a coexistence of the LE and liquid condensed (LC) phases. This transition is also observed for pure DPPC monolayers.

Further compression leads to a plateau in the isotherm (typically between 40 and 55 mN/m), the significance of which is highly debated. While some consider it representative of a selective molecular squeeze-out, where non-DPPC molecules are removed from the interface as the film progresses to highly compressed states (*44*), others believe that the plateau corresponds to protein-induced, organized reversible structural squeeze-out. In this protein-induced squeeze-out, SP-B facilitates the formation of folded, three-dimensional film structures close to the interface that promote stability of the highly compressed film. SP-B would also participate in the unfolding of these structures, thereby increasing respreadability during film expansion (*3, 45*). A good LS replacement is expected to exhibit a pronounced plateau in this region (*43*). Upon further compression of the barriers, the monolayer becomes a solid phase and finally reaches collapse. Good LS replacements typically have a collapse pressure near 72 mN/m, corresponding to near-zero surface tension (*43*).

The surfactant films studied here all exhibit high collapse pressures of ~72 mN/m. The lipid-only film has a lift-off area of ~100 Å^2/molecule and a small kink at ~55 mN/m. With the addition of SP-B$_{1-25}$, an earlier lift-off of ~120 Å^2/molecule is observed, indicating that the presence of the peptide at the interface alters the available area per molecule and causes the lipids to begin interacting with one another at a larger molecular area. In addition, a much more distinct plateau is observed at ~50 mN/m. The **B1**/lipid film has a lift-off area intermediate between that of the lipid and that of SP-B$_{1-25}$/lipid films (~110 Å^2/molecule) and an even more pronounced plateau than the SP-B$_{1-25}$/lipid film. The lipid film with the aromatic insertion region-containing peptoid, **B3**, exhibits a similar lift-off area of ~110 Å^2/molecule and a less extensive plateau, more similar to that of the SP-B$_{1-25}$/lipid film. Hence, by this test, the inclusion of a hydrophobic insertion region at the N-terminus does not seem to greatly affect the in vitro surface activity of aromatic peptoid-based mimics of SP-B$_{1-25}$.

The aliphatic peptoids (**B4**, **B5**, and **B6**) provided slightly earlier lift-off areas than the aromatic peptoids (~115, ~125, and ~125 Å^2/molecule, respectively) but exhibited much less defined plateaus in the isotherm at ~50 mN/m. In the case of the aliphatic peptoids, those that contain an N-terminal insertion region show an earlier lift-off, where the lipid/peptoid films begin to form an organized structure at larger molecular areas. Furthermore, there seems to be little difference between the isotherms for **B5** and **B6** in the plateau
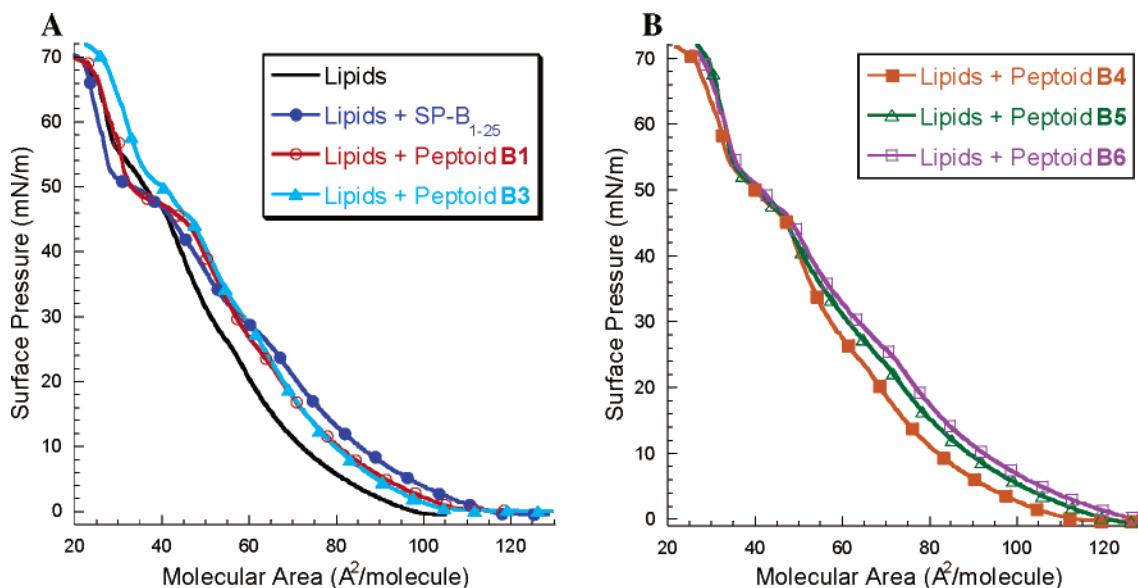
FIGURE 2: Π−*A* isotherms for lipids alone (A, black), lipids with 2.16 mol % SP-B$_{1−25}$ (A, blue, filled circles), lipids with 2.16 mol % peptoid **B1** (A, red, empty circles), lipids with 2.16 mol % peptoid **B3** (A, light blue, filled triangles), lipids with 2.16 mol % peptoid **B4** (B, orange, filled squares), lipids with 2.16 mol % peptoid **B5** (B, green, empty triangles), and lipids with 2.16 mol % peptoid **B6** (B, purple, empty squares) in buffer at 37 °C with a barrier speed of 30 mm/min.
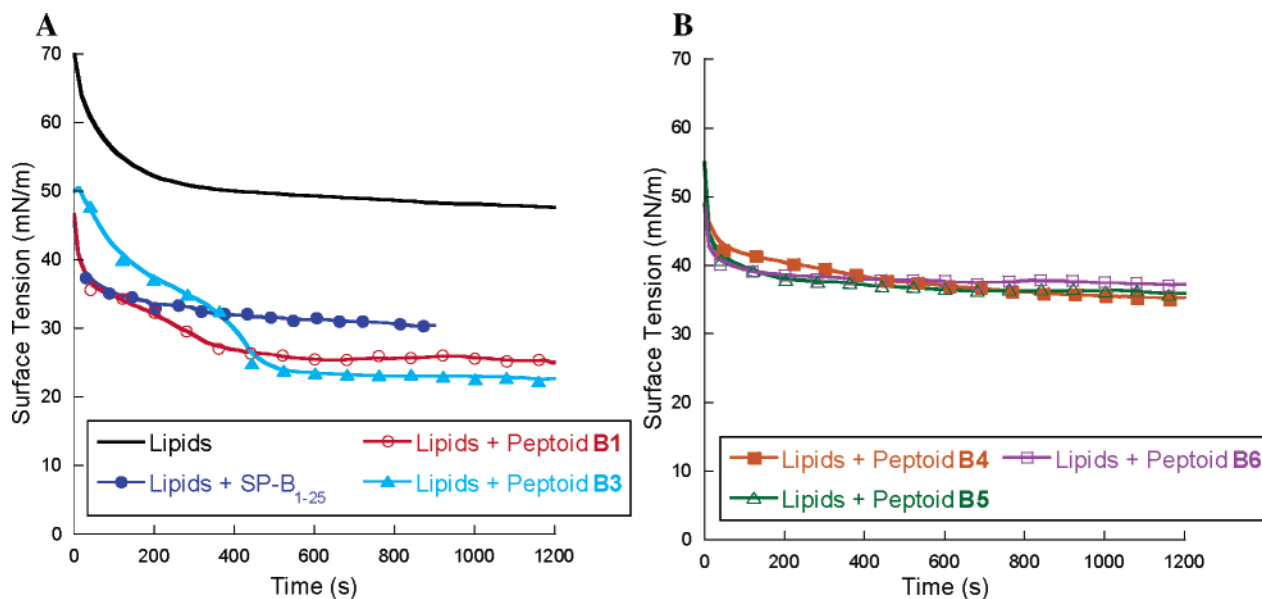

FIGURE 3: Static adsorption data for lipids alone (A, black), lipids with 2.16 mol % SP-B$_{1−25}$ (A, blue, filled circles), lipids with 2.16 mol % peptoid **B1** (A, red, empty circles), lipids with 2.16 mol % peptoid **B3** (A, light blue, filled triangles), lipids with 2.16 mol % peptoid **B4** (B, orange, filled squares), lipids with 2.16 mol % peptoid **B5** (B, green, empty triangles), and lipids with 2.16 mol % peptoid **B6** (B, purple, empty squares) in buffer at 37 °C.

region, indicating that the substitution of NLys for NArg does not affect surface activity (by this test). While the aromatic peptoids, **B1** and **B3**, have a later lift-off area, they exhibit more pronounced plateaus than the aliphatic peptoids, which may be due to their more stable helical structures and/ or to their improved ability to facilitate lipid interactions at highly compressed surfactant states.

Static-Bubble Pulsating Bubble Surfactometry. The adsorption kinetics of the peptide- and peptoid-based mimics were investigated in a lipid film [68/22/9 DPPC/POPG/PA mixture (w/w)] at 37 °C, using a pulsating bubble surfactometer (PBS) in static-bubble mode (Figure 3). A bubble with a radius of 0.4 mm was formed, and surface tension data were recorded continuously for 20 min or until equi-

librium surface tension was reached. A good LS replacement is expected to reach an equilibrium surface tension of approximately 25 mN/m very rapidly, within 1−2 min (*46*). These studies reveal that the lipid mixture with no additives has a relatively high equilibrium surface tension (∼48 mN/ m) and takes a long time to reach equilibrium, nearly 20 min. The addition of 2.16 mol % SP-B$_{1−25}$ resulted in a lower equilibrium surface tension of ∼30 mN/m that was reached much more quickly, within ∼10 min. The lipid films containing aromatic peptoids **B1** and **B3** showed improved surface activity over both lipids alone and the SP-B$_{1−25}$/lipid film, with low equilibrium surface tensions of ∼25 and ∼23 mN/m, respectively, reached after only ∼5 min in the case of **B1** and 7 min in the case of **B3**. Intriguingly, SP-B$_{1−25}$,
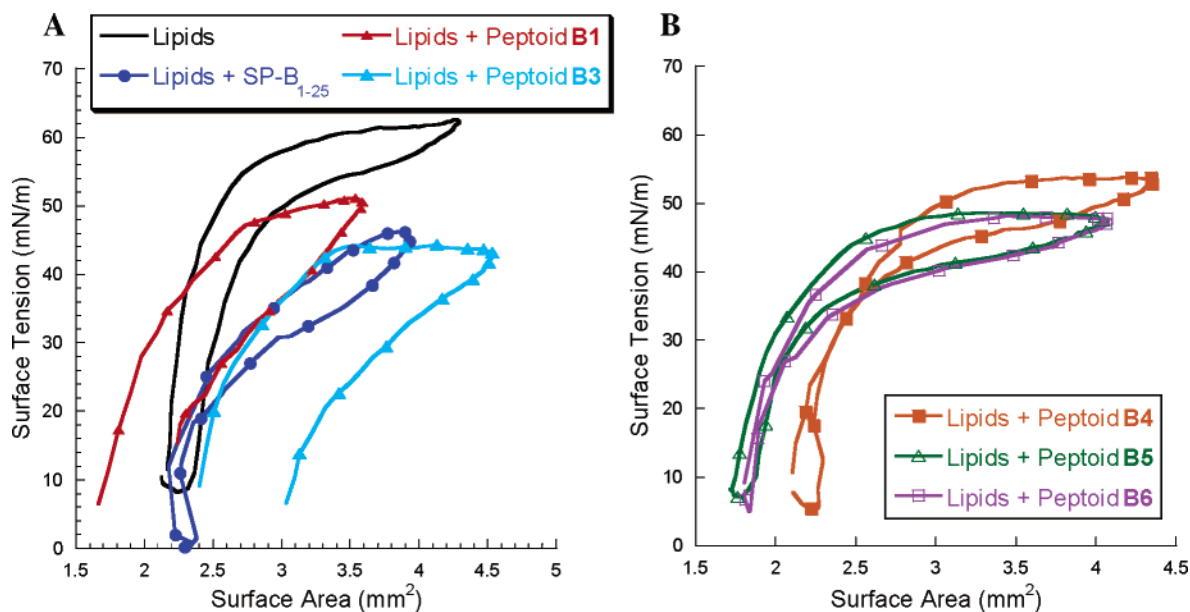
FIGURE 4: Dynamic adsorption data for lipids alone (A, black), lipids with 2.16 mol % SP-B$_{1-25}$ (A, blue, filled circles), lipids with 2.16 mol % peptoid **B1** (A, red, filled triangles), lipids with 2.16 mol % peptoid **B3** (A, light blue, filled triangles), lipids with 2.16 mol % peptoid **B4** (B, orange, filled squares), lipids with 2.16 mol % peptoid **B5** (B, green, empty triangles), and lipids with 2.16 mol % peptoid **B6** (B, purple, empty squares) in buffer at 37 °C with a pulsation rate of 20 cycles/min.

B1, and **B3** all exhibit a two-step adsorption to the air–aqueous interface in the static-bubble mode on the PBS. This phenomenon has been noted by other researchers for natural SP-B (*9, 47, 48*) and is thought to represent an initial, slow adsorption of surfactant to the clean interface, followed by an inflection and more rapid adsorption of additional molecules to the existing surfactant film to the final equilibrium surface tension. We have not yet determined the sequence and structural features of the peptoid mimics that lead to two-step adsorption but will explore this further with future designs. It should be noted, however, that while this occurs with natural SP-B, whole CLSE does not exhibit two-step adsorption kinetics but adsorbs extremely rapidly to a low equilibrium surface tension.

The aliphatic peptoids, **B4**, **B5**, and **B6**, had slightly higher equilibrium surface tensions of ~35 mN/m. The insertion region-containing peptoids, **B5** and **B6**, exhibited much more rapid adsorption to the interface, only ~2 min, compared to that of the **B4**/lipid film, ~10 min. We hypothesize that peptoids **B5** and **B6** enhance the rate of surfactant adsorption to the air–liquid interface due to the interaction of their aliphatic insertion regions with the acyl lipid tails, anchoring them into the monolayer. However, the peptoids composed of chiral, aromatic side chains, especially **B3**, are able to reach a lower equilibrium surface tension, albeit with a less rapid adsorption rate. It is also interesting to note that there appears to be no difference in surfactant adsorption for films containing **B5** or **B6**, suggesting that arginine is not an essential residue for good surface activity in a peptoid-based mimic of SP-B$_{1-25}$.

Dynamic-Bubble Pulsating Bubble Surfactometry. To assess the surface-active behavior of the surfactant formulations during film area cycling, dynamic-bubble PBS experiments were performed at 37 °C (Figure 4). A bubble with a radius of 0.4 mm was formed and then dynamically cycled at a frequency of 20 cycles/min until equilibrium was reached (i.e., until no further changes in maximum and minimum

surface tension were detected). The surface area and surface tension were both calculated at a rate of 10–20 data points per minute. The data are presented in the form of hysteresis loops (surface area vs surface tension); the loop direction is clockwise. The hysteresis loop for natural LS is expected to exhibit a low maximum surface tension of ~35 mN/m, a near-zero surface tension upon compression, and a high degree of hysteresis, indicating that only a small amount of film compression is required to reach the minimum surface tension (*46, 49*). Upon compression, the lipid film transitions from a monolayer to multilayer structure, as material is removed from the interface to allow the surface tension to reach nearly zero. Because the image analysis system on our modified PBS instrument calculates both surface area and surface tension using information obtained from fitting the bubble with an ellipse, if the bubble shape deforms from that of an ellipse (as it frequently does at near-zero surface tensions), surface area and surface tension cannot be calculated. Therefore, there are no data points on the hysteresis loops in these regions (Figure 4A, **B1** and **B3**). Additionally, the bubble size was not adjusted throughout the run so that the adsorption kinetics were not adversely affected. Although this led to the horizontal shifts of the PBS data loops, such as that observed between lipids and the **B1**/lipid film in Figure 4A, this has no effect on the overall surface activity.

The hysteresis loop for the lipid film with no SP-B mimics reveals a high maximum surface tension (~60 mN/m), a relatively high minimum surface tension (~10 mN/m), and a very low level of loop hysteresis. The addition of the SP-B$_{1-25}$ peptide results in a lower maximum surface tension (~45 mN/m) and attainment of a near-zero minimum surface tension, and while significant bubble deformation was observed, the extent of loop hysteresis was small. The **B1**/lipid film has a slightly higher maximum surface tension than the SP-B$_{1-25}$/lipid film (~50 mN/m) but still reaches near-zero surface tension and has significantly more hysteresis.

The addition of **B3** to the lipid film results in a maximum surface tension slightly lower than that of SP-B$_{1-25}$ or **B1** ($\sim$43 mN/m), a near-zero minimum surface tension, and a high degree of hysteresis, similar to that of the **B1**/lipid film. The aliphatic peptoids, **B4**, **B5**, and **B6**, all induce only small extents of hysteresis, like SP-B$_{1-25}$, but still reach near-zero minimum surface tensions. While the **B4**/lipid film has a maximum surface tension slightly higher than that of **B1** ($\sim$52 mN/m) and a small extent of hysteresis, both the **B5**/lipid and **B6**/lipid films exhibit lower maximum surface tensions of $\sim$48 mN/m. Therefore, the addition of the insertion region to the peptoid-based mimics (aromatic or aliphatic) results in a lower maximum surface tension. While the physiological importance of the maximum surface tension is unknown, it is accepted that natural LS has a low maximum surface tension of $\sim$35 mN/m. The insertion region-containing surfactant formulations do not reach this value, but they do reach a maximum surface tension close to, or in the case of **B3** better than, that of the SP-B$_{1-25}$/lipid film. Additionally, we have shown that the substitution of arginine for lysine does not significantly affect the surface-active behavior. The aromatic peptoids, **B1** and **B3**, exhibit much larger extents of hysteresis than the aliphatic peptoids, **B4**, **B5**, and **B6**. It is likely that the more stable helix formed by the aromatic side chains is better able to interact with the lipid monolayer and enhance the rapid decrease to near-zero surface tension upon a small amount of film compression. This phenomenon is not yet well understood but will be further investigated using molecular dynamic simulations as well as X-ray studies of peptoids within mixed lipid films.

We have further evaluated the dynamic PBS data by comparing the duration of cycling required to reach near-zero surface tension and the extent of compression required for minimum surface tension changed throughout cycling (data not shown). The SP-B$_{1-25}$ film, and the aromatic peptoid-containing films, all reached their minimum surface tensions on the first cycle. On the other hand, the aliphatic peptoid-containing films required 1−10 min to establish an equilibrium minimum surface tension. While the SP-B$_{1-25}$ film exhibited a progressive decrease in the amount of compression required to reach the minimum surface tension, the aromatic peptoid-containing films immediately reached near-zero surface tension with an only small amount of compression. The aliphatic peptoid-containing films required 5−10 min to establish the amount of compression required for minimum surface tension. As expected from evaluation of the equilibrium hysteresis loops, the aromatic peptoid-containing films exhibit significantly more biomimetic surface-active behavior than the aliphatic peptoid-containing films. In addition, they are able to reach equilibrium immediately, like natural LS.

CONCLUSIONS

We have designed, characterized, and evaluated the in vitro surface activity of peptoid-based mimics of SP-B$_{1-25}$ that include a hydrophobic, helical, N-terminal insertion region (residues 1−9) and two arginine-like side chains in the C-terminal helix, two structural features that are present in SP-B$_{1-25}$ and that have previously been demonstrated as being important for its function. The hydrophobic insertion region has been found to insert into the lipid layer and interact with the acyl chains, and previous studies have

shown that truncated versions of this peptide or variants that lack amino acids with ring structures (proline, tryptophan, and tyrosine) exhibit significantly decreased surface tension reducing properties (*24, 25, 38*). The two arginine side chains in SP-B$_{1-25}$ are also considered to be important because they interact with both the anionic (POPG) and zwitterionic (DPPC) lipid head groups in the lipid layer (*28*). However, the inclusion of arginine-like side chains in peptoids is problematic due to the low solubility of the PMC-protected submonomer under reaction conditions, as well as difficulty in removing the PMC protecting group without side chain degradation during cleavage. The substitution of lysine-like side chains for arginine-like side chains in peptoids makes them much easier to synthesize and purify in high yield.

All molecules studied had helical CD spectra, as expected for the respective classes of helices. In general, increased spectral intensity corresponds to greater helix stability, and results indicate that (i) both aromatic and aliphatic peptoids form stable helices and (ii) the substitution of NArg for NLys in the amphipathic helix of the aliphatic peptoids does not alter secondary structure or helix stability. Such stability may play a critical role in lipid−peptoid interactions at the air−liquid interface.

The surface activity differences in aromatic- versus aliphatic-containing peptoids may provide insight into their ability to facilitate the desired lipid dynamics in interfacial films. The increased lift-off areas observed on the LWSB with aliphatic peptoids when compared to those of aromatic peptoids may be explained by the less stable, more flexible helices formed by the less bulky, Nssb side chains (*42*). These molecules would occupy a greater fraction of the area at the interface in the gaseous phase, leading to lipid interactions at earlier molecular areas. Furthermore, increasing the number of residues in the aliphatic-containing peptoids, and thus the length of the helix, through the addition of an insertion region resulted in increased lift-off areas relative to the shorter **B4**. The more stable helices formed by aromatic-containing peptoids would presumably occupy less space, and accordingly, later lift-off areas are observed as compared to those of the aliphatic peptoids. However, it is interesting to note that helical length does not seem to affect lift-off area in aromatic peptoids and actually decreases spectral helical intensity. On the basis of these results, the area occupied by peptoids at the interface may not be the sole factor that determines lift-off area values. Instead, overall lipid−peptoid interactions and total organization of the surfactant film in the gaseous phase may play a greater role in this initial increase in surface pressure. In the plateau region, the significantly less pronounced plateau exhibited by aliphatic peptoids when compared to aromatic peptoids may be the result of a differing ability to organize or stabilize the surfactant film at higher surface pressures. If the presence of a more pronounced plateau signifies a higher degree of film reorganization into stable, folded, three-dimensional structures, it appears that aromatic peptoids have an enhanced ability to more effectively manage the film during highly compressed states.

Interestingly, in addition to promoting earlier lipid−peptoid interactions in the gaseous phase on the LWSB, the aliphatic peptoids are also able to adsorb more rapidly to the air−liquid interface of a bubble than the aromatic peptoids, as determined using a PBS. The less bulky, more

flexible helices of the aliphatic peptoids may more easily interact with lipids in uncompressed states, promoting more rapid adsorption and crude organization. However, the stable helices of aromatic peptoids appear to be better able to facilitate the necessary lipid dynamics after initial adsorption has taken place, leading to a lower equilibrium surface tension. The dynamic-bubble PBS data further support this theory by showing that aromatic peptoids are better able to interact with lipids during highly compressed states, with less compression required to reach minimum surface tensions, and an increased level of hysteresis. Aromatic peptoids also seem to maintain lipid organization at bubble expansion more efficiently than aliphatic peptoids, as demonstrated by lower maximum surface tensions.

Clearly, the inclusion of an N-terminal, hydrophobic insertion region and the proper placement of the cationic side chains in peptoids **B3**, **B5**, and **B6** do significantly improve their in vitro surface activities, by comparison of these more biomimetic peptoids to our first generation of simple, helical, amphipathic peptoid mimics of SP-B$_{1-25}$. Note that our study is able to provide only an aggregate comparison of the importance of these two distinct structural features, since they were not investigated separately. The presence of a hydrophobic, helical segment promotes an increased level of insertion into and interactions with lipid tails, leading to enhanced surface activity. In both the aromatic- and aliphatic-containing peptoids, the presence of an insertion region significantly improved the peptoids' ability to maintain lower surface tensions at bubble expansion. The anchoring of the peptoid helices to an expanding lipid film may result in enhanced respreadability, as well as facilitate lipid transport and organization. Extending the helix through addition of an insertion region may further accentuate trends in surface activity that are already present, such as rapid adsorption, if they are mainly affected by secondary structure characteristics such as helix stability and rigidity. Recently, it was demonstrated that removal of ring-containing amino acids in the insertion region of the SP-B peptide mimics significantly decreased surface-active behavior, and investigation into the impact of these residues on surface activity in peptoids will continue to be explored (*24, 25*). In addition, these studies show that the substitution of lysine-like side chains for arginine-like side chains in peptoids (**B5** vs **B6**) does not affect the surface-active behavior of the surfactant film. It is likely that the presence of multiple cationic charges in an amphipathic helix is more crucial to surface activity than the side chain structures. This result is beneficial for the future syntheses of Nspe-containing peptoid sequences that could not be purified in the presence of PMC-protected NArg.

The sequences of the peptoids studied here are relatively similar to each other, with small differences in cationic side chain placement and hydrophobic side chain chemistry. However, these seemingly minor sequence alterations result in significant variations in surface activity. It is also interesting to note that relative lipophilicity, as judged by RP-HPLC retention time, does not seem to correlate in any simple way with surface-active behavior. For example, our two most hydrophobic peptoids, **B3** and **B6**, which have very similar hydrophobicities, exhibit substantial differences in their surface activities determined by all in vitro techniques used in this study. However, one of our best mimics, by

several measures, is **B3**, a peptoid that has an average hydrophobicity essentially equal to that of SP-B$_{1-25}$. The correlation of surface activity with overall helicity is similarly difficult to assess, since all peptoids have overall helical structures (note that **B3** is one of the least helical peptoids).

The studies presented here demonstrate that it is possible to create SP mimics with excellent surface activities, through the careful design of peptoid sequences that are more similar to that of the natural SP-B$_{1-25}$ peptide, with biomimetic sequence patterning in terms of the positioning of hydrophobic and cationic monomers. Peptoids **B5** and **B6** exhibit the best surface activity by LWSB studies and have the most rapid adsorption rates on the PBS, while **B3** reaches the lowest equilibrium surface tension and has by far the most hysteresis in the PBS data loop. All of these attributes would be desirable in a single mimic, which indicates that more work remains to be done. At this point in the field of lung surfactant science, it is unclear which of these individual in vitro surface-active behaviors is most critical for in vivo efficacy; however, it is interesting that these specific behaviors seem to correlate with peptoid sequence and structure. Presumably, however, it will be best to create a biomimetic surfactant replacement that closely mimics all of the unique surface-active properties of whole, natural lung surfactant, and admittedly, we and the LS research community still have a long way to go to achieve this with a non-natural material. However, the results of this study lead us to believe that sequence-specific peptoids are an ideal template for the correlation of SP-mimic structural attributes with the characteristic activities exhibited by natural surfactant proteins.

ACKNOWLEDGMENT

REFERENCES

1. Frerking, I. (2001) Pulmonary surfactant: Functions, abnormalities and therapeutic options, *Intensive Care Med. 27*, 1699−1717.
2. Notter, R. H. (2000) *Lung Surfactants: Basic Science and Clinical Applications*, Vol. 149, Marcel Dekker, New York.
3. Serrano, A. G., and PerezGil, J. (2006) Protein-lipid interactions and surface activity in the pulmonary surfactant system, *Chem. Phys. Lipids 141*, 105−118.
4. Goerke, J., and Clements, J. A. (1986) in *Handbook of Physiology. Section 3, The Respiratory System. Volume 3, Mechanics of Breathing: Part I* (Fishman, A., Macklem, P., Mead, J., and Geiger, S., Eds.) pp 247−262, American Physiological Society, Bethesda, MD.
5. Goerke, J. (1997) Pulmonary surfactants: Physicochemical aspects, *Curr. Opin. Colloid Interface Sci. 2*, 526−530.
6. McLean, L. R., and Lewis, J. E. (1995) Biomimetic pulmonary surfactants, *Life Sci. 56*, 363−378.
7. Veldhuizen, R., Nag, K., Orgeig, S., and Possmayer, F. (1998) The role of lipids in pulmonary surfactant, *Biochim. Biophys. Acta 1408*, 90−108.
8. Hall, S. B., Venkitaraman, A. R., Whitsett, J. A., Holm, B. A., and Notter, R. H. (1992) Importance of hydrophobic apoproteins as constituents of clinical exogenous surfactants, *Annu. Rev. Respir. Distress 145*, 24−30.
9. Wang, Z., Hall, S. B., and Notter, R. H. (1996) Roles of different hydrophobic constituents in the adsorption of pulmonary surfactant, *J. Lipid Res. 37*, 790−798.

10. Creuwels, L., Demel, R. A., Vangolde, L. M. G., and Haagsman, H. P. (1995) Characterization of a Dimeric Canine Form of Surfactant Protein C(Sp-C), *Biochim. Biophys. Acta 1254*, 326–332.

11. Clark, J. C., Wert, S. E., Bachurski, C. J., Stahlman, M. T., Stripp, B. R., Weaver, T. E., and Whitsett, J. A. (1995) Targeted Disruption of the Surfactant Protein-B Gene Disrupts Surfactant Homeostasis, Causing Respiratory-Failure in Newborn Mice, *Proc. Natl. Acad. Sci. U.S.A. 92*, 7794–7798.

12. Glasser, S. W., Burhans, M. S., Korfhagen, T. R., Na, C.-L., Sly, P. D., Ross, G. F., Ikegami, M., and Whitsett, J. A. (2001) Altered stability of pulmonary surfactant in SP-C-deficient mice, *Proc. Natl. Acad. Sci. U.S.A. 98*, 6366–6371.

13. Beck, D. C., Ikegami, M., Na, C. L., Zaltash, S., Johansson, J., Whitsett, J. A., and Weaver, T. E. (2000) The role of homodimers in surfactant protein B function in vivo, *J. Biol. Chem. 275*, 3365–3370.

14. Johansson, J., Curstedt, T., and Jornvall, H. (1991) Surfactant protein B: Disulfide bridges, structural properties, and kringle similarities, *Biochemistry 30*, 6917–6921.

15. Nogee, L. M. (2004) Alterations in SP-B and SP-C expression in neonatal lung disease, *Annu. Rev. Physiol. 66*, 601–623.

16. Wustneck, N., Wustneck, R., Perez-Gil, J., and Pison, U. (2003) Effects of oligomerization and secondary structure on the surface behavior of pulmonary surfactant proteins SP-B and SP-C, *Biophys. J. 84*, 1940–1949.

17. Krol, S., Janshoff, A., Ross, M., and Galla, H.-J. (2000) Structure and function of surfactant protein B and C in lipid monolayers: A scanning force microscopy study, *Phys. Chem. Chem. Phys. 2*, 4586–4593.

18. Gordon, L. M., Horvath, S., Longo, M. L., Zasadzinski, J. A. N., Taeusch, H. W., Faull, K., Leung, C., and Waring, A. J. (1996) Conformation and molecular topography of the N-terminal segment of surfactant protein B in structure-promoting environments, *Protein Sci. 5*, 1662–1675.

19. Veldhuizen, E. J. A., Batenburg, J. J., Golde, L. M. G. v., and Haagsman, H. P. (2000) The role of surfactant proteins in DPPC enrichment of surface films, *Biophys. J. 79*, 3164–3171.

20. Baatz, J. E., Sarin, V., Absolom, D. R., Baxter, C., and Whitsett, J. A. (1991) Effects of Surfactant-Associated Protein SP-B Synthetic Analogs on the Structure and Surface-Activity of Model Membrane Bilayers, *Chem. Phys. Lipids 60*, 163–178.

21. Bruni, R., Taeusch, H. W., and Waring, A. J. (1991) Surfactant protein B: Lipid interactions of synthetic peptides representing the amino-terminal amphipathic domain, *Proc. Natl. Acad. Sci. U.S.A. 88*, 7451–7455.

22. Lipp, M. M., Lee, K. Y. C., Zasadzinski, J. A., and Waring, A. J. (1997) Solving medical problems with chemical engineering, *CHEMTECH 27*, 42–57.

23. Longo, M. L., Bisagno, A. M., Zasadzinski, J. A. N., Bruni, R., and Waring, A. J. (1993) A Function of Lung Surfactant Protein Sp-B, *Science 261*, 453–456.

24. Ryan, M. A., Qi, X., Serrano, A. G., Ikegami, M., PerezGil, J., Johansson, J., and Weaver, T. E. (2005) Mapping and Analysis of the Lytic and Fusogenic Domains of Surfactant Protein B, *Biochemistry 44*, 861–872.

25. Serrano, A. G., Ryan, M. A., Weaver, T. E., and PerezGil, J. (2006) Critical Structure-Function Determinants within the N-Terminal Region of Pulmonary Surfactant Protein B, *Biophys. J. 90*, 238–249.

26. Lee, K. Y. C., Majewski, J., Kuhl, T. L., Howes, P., Kjaer, K., Lipp, M. M., Waring, A., Zasadzinski, J. A., and Smith, G. S. (2000) The incorporation of lung surfactant specific protein SP-B into lipid monolayers at the air-fluid interface: A grazing incidence X-ray diffraction study, *Mater. Res. Soc. Symp. Proc. 590*, 177–182.

27. Lee, K. Y. C., Majewski, J., Kuhl, T. L., Howes, P. B., Kjaer, K., Lipp, M. M., Waring, A. J., Zasadzinski, J. A., and Smith, G. S. (2001) Synchroton X-ray study of lung surfactant-specific protein SP-B in lipid monolayers, *Biophys. J. 81*, 572–585.

28. Kaznessis, Y. N., Kim, S., and Larson, R. G. (2002) Specific mode of interaction between components of model pulmonary surfactants using computer simulations, *J. Mol. Biol. 322*, 569–582.

29. Simon, R. J., Kania, R. S., Zuckermann, R. N., Huebner, V. D., Jewell, D. A., Banville, S., Ng, S., Wang, L., Rosenberg, S., et al. (1992) Peptoids: A modular approach to drug discovery, *Proc. Natl. Acad. Sci. U.S.A. 89*, 9367–9371.

30. Zuckermann, R. N., Kerr, J. M., Kent, S. B. H., and Moos, W. H. (1992) Efficient method for the preparation of peptoids [oligo-(N-substituted glycines)] by submonomer solid-phase synthesis, *J. Am. Chem. Soc. 114*, 10646–10647.

31. Armand, P., Kirshenbaum, K., Goldsmith, R. A., Farr-Jones, S., Barron, A. E., Truong, K. T. V., Dill, K. A., Mierke, D. F., Cohen, F. E., Zuckermann, R. N., and Bradley, E. K. (1998) NMR determination of the major solution conformation of a peptoid pentamer with chiral side chains, *Proc. Natl. Acad. Sci. U.S.A. 95*, 4309–4314.

32. Seurynck, S. L., Patch, J. A., and Barron, A. E. (2005) Simple, helical peptoid analogs of lung surfactant protein B, *Chem. Biol. 12*, 77–88.

33. Seurynck, S. L., Brown, N. J., Wu, C. W., Germino, K. W., Kohlmeir, E. K., Ingenito, E. P., Glucksberg, M. R., Barron, A. E., and Johnson, M. (2005) Optical monitoring of bubble size and shape in a pulsating bubble surfactometer, *J. Appl. Physiol. 99*, 624–633.

34. Krapcho, A. P., and Kuell, C. S. (1990) Mono-Protected Diamines: N-tert-Butoxycarbonyl-α,ω-Alkanediamines from α,ω-Alkanediamines, *Synth. Commun. 20*, 2559–2564.

35. Uno, T., Beausoleil, E., Goldsmith, R. A., Levine, B. H., and Zuckermann, R. N. (1999) New submonomers for poly N-substituted glycines (peptoids), *Tetrahedron Lett. 40*, 1475–1478.

36. Tanaka, Y., Takei, T., Aiba, T., Masuda, K., Kiuchi, A., and Fujiwara, T. (1986) Development of synthetic lung surfactants, *J. Lipid Res. 27*, 475–485.

37. Putz, G., Goerke, J., Taeusch, H. W., and Clements, J. A. (1994) Comparison of captive and pulsating bubble surfactometers with use of lung surfactants, *J. Appl. Physiol. 76*, 1425–1431.

38. Kurutz, J. W., Diamant, H., Jiarpinitnun, C., Waring, A., and Lee, K. Y. C. (2005) in *Lung Surfactant Function and Disorder* (Nag, K., Ed.) Marcel Dekker, New York.

39. Kirshenbaum, K., Barron, A. E., Goldsmith, R. A., Armand, P., Bradley, E. K., Truong, K. T. V., Dill, K. A., and Cohen, F. E. (1998) Sequence-specific polypeptoids: A diverse family of heteropolymers with stable secondary structure, *Proc. Natl. Acad. Sci. U.S.A. 95*, 4303–4308.

40. Wu, C. W., Sanborn, T. J., Huang, K., Zuckermann, R. N., and Barron, A. (2001) Peptoid oligomers with α-chiral, aromatic side chains: Sequence requirements for the formation of stable peptoid helices, *J. Am. Chem. Soc. 123*, 6778–6784.

41. Wu, C. W., Sanborn, T. J., Zuckermann, R. N., and Barron, A. (2001) Peptoid oligomers with α-chiral, aromatic side chains: Effects of chain length on secondary structure, *J. Am. Chem. Soc. 123*, 2958–2963.

42. Wu, C. W., Kirshenbaum, K., Sanborn, T. J., Patch, J. A., Huang, K., Dill, K. A., Zuckermann, R. N., and Barron, A. E. (2003) Structural and spectroscopic studies of peptoid oligomers with α-chiral aliphatic side chains, *J. Am. Chem. Soc. 125*, 13525–13530.

43. Alonso, C., Alig, T., Yoon, J., Bringezu, F., Warriner, H., and Zasadzinski, J. A. (2004) More than a monolayer: Relating lung surfactant structure and mechanics to composition, *Biophys. J. 87*, 4188–4202.

44. Flanders, B. N., Vickery, S. A., and Dunn, R. C. (2001) Imaging of monolayers composed of palmitic acid and lung surfactant protien B, *J. Microsc. 202*, 379–385.

45. Cruz, A., Worthman, L. A., Serrano, A. G., Casals, C., Keough, K. M. W., and Perez-Gil, J. (2000) Microstructure and dynamic surface properties of surfactant protein SP-B/dipalmitoylphosphatidylcholine interfacial films spread from lipid-protein bilayers, *Eur. Biophys. J. 29*, 204–213.

46. Scarpelli, E. M., David, E., Cordova, M., and Mautone, A. J. (1992) Surface-Tension of Therapeutic Surfactants (Exosurf Neonatal, Infasurf, and Survanta) as Evaluated by Standard Methods and Criteria, *Am. J. Perinatol. 9*, 414–419.

47. Schram, V., and Hall, S. B. (2001) Thermodynamic Effects of the Hydrophobic Surfactant Proteins on the Early Adsorption of Pulmonary Surfactant, *Biophys. J. 81*, 1536–1546.

48. Walters, R. W., Jenq, R. R., and Hall, S. B. (2000) Distinct steps in the adsorption of pulmonary surfactant to an air-liquid interface, *Biophys. J. 78*, 257–266.

49. Ingenito, E. P., Morris, L. M. J., Espinosa, F. F., Kamm, R. D., and Johnson, M. (1999) Biophysical characterization and modeling of lung surfactant components, *J. Appl. Physiol. 86*, 1702–1714.